Blind Matched Filter Design for Communication Chains Involving Frequency Multipliers: LSTM-based Approach

Ahmet Alperen Oznam*, Mohaned Chraiti*‡, Ali Ghrayeb†, Korkut Kaan Tokgöz*
*Faculty of Engineering and Natural Sciences, Sabancı University, İstanbul, Türkiye.
†College of Science and Engineering, Hamad Bin Khalifa University, Doha, Qatar.
‡DGTL X, Kocaeli, Turkey
Emails: aoznam@sabanciuniv.edu, mohaned.chraiti@sabanciuniv.edu, aghrayeb@hbku.edu.qa, and korkut.tokgoz@sabanciuniv.edu

***Abstract*—Frequency multipliers are increasingly utilized for signal up-conversion in modern wireless communication systems, particularly in millimeter-wave (mmWave) and sub-terahertz (sub-THz) bands, owning to their simplicity and ease of integration. However, their inherent nonlinearity causes distortions, fundamentally altering the temporal and spectral characteristics of transmitted signals. This distortion transforms well-defined baseband pulses (e.g., sinc, raised cosine) into complex, hardware-dependent waveforms, where the matched-filter depends both on the multiplication order and the specific hardware implementation. Notably, the spectral occupancy of the transmitted signal expands after frequency multiplication. Without accurate knowledge of the multiplier-induced distortions at the receiver, applying a mismatched filter can cause severe inter-symbol interference and loss of critical frequency components, signal-to-noise ratio degradation thereby degrading detection performance. In this paper, we propose a blind, adaptive matched-filter estimation approach leveraging a Long Short-Term Memory (LSTM) neural network. Our method directly estimates the matched filter from sampled segments of the noisy modulated received signal without requiring pilot symbols. The proposed model adapts to dynamic pulse shapes and amplitudes by implicitly learning the spectral transformations introduced by hardware-induced nonlinearities. Simulation results demonstrate high accuracy of the matched filter estimation, with a mean-square error precision of four decimal places.**

***Index Terms*—Adaptive filtering, frequency multipliers, LSTM, matched filters, mmWave communications.**

I. INTRODUCTION

The demand for Gigabit/s wireless links and massive connectivity is rapidly increasing. Seeking solutions, both the wireless industry and academia are continuously exploring millimeter-wave (mmWave) and Sub-Terahertz (Sub-THz) bands, which offer bandwidths in the gigahertz range. Up-converting the signal to mmWave and Sub-THz bands is deemed to be a challenging task due to hardware limitations. In the sub-6 GHz band, a sequence of mixers is typically used for up-conversion, where the input signal is sequentially multiplied by single-tone waveforms generated from local oscillators. However, at higher frequencies, mixers suffer from conversion losses, high noise, and increased cost. Circuit designers are compelled to rely more on passive components for signal up-conversion and develop novel architectures involving frequency multipliers [1]–[4]. The proposed architecture involves passing an intermediate frequency's modulated signal, centered around low-frequency carrier, through a frequency multiplier, rather than a sequence of mixers. Leveraging electronic components with non-linear behavior, it is possible to generate multiple harmonics from an input signal, which can then be selectively filtered to obtain the desired high-frequency output [1], [3]. The study in [1] demonstrates the feasibility of achieving 16 Gbps transmission at 240 GHz, highlighting the efficacy of frequency multipliers for up-conversion.

Despite their advantages, frequency multipliers introduce challenges that can compromise, if not addressed, the reliability and efficiency of communication systems. Principally, their inherent nonlinearity, while essential for carrier up-conversion, results in pulse shape non-linear distortion. In the frequency domain, this manifests as bandwidth expansion, where the signal's spectral support expands. In the time domain, the effect appears as a reshaping of the pulse and a reduction in the pulse width [3], [5], [6]. Consequently, the spectral and temporal profile of the transmitted signal no longer align with the original baseband waveform, and the degree of distortion depends on the order and configuration of the frequency multiplier. Importantly, even basic pulse shapes such as sinc or raised cosine pulses become distorted into non-standard formats after passing through frequency multipliers. The resulting waveform characteristics are determined not only by the multiplication factor but also by the specific cascade configuration used in the hardware. For instance, a signal intended for transmission at 60 GHz could be generated by up-converting a 10 GHz intermediate frequency followed by a doubler and a tripler, or alternatively, by up-converting to 5 GHz followed by a quadruplicator and a tripler. Although these configurations yield the same output frequency, the spectral and temporal characteristics of the resulting signal

This project has received funding from the European Union's Horizon 2020 research and innovation program under the Marie Sklodowska-Curie grant agreement No 101108094. This work is supported by Tübitak under grant 122E497.

can differ significantly due to their internal structure. These hardware-specific configurations are typically not shared with the receiver, as they are not part of existing communication standards. Furthermore, communicating such specifications would introduce additional overhead and complexity, which is generally avoided in practice. These introduce uncertainty in the received signal format, particularly affecting the design and application of matched filters.

The matched filter is a fundamental component in digital communication receivers, designed to maximize the signal-to-noise ratio (SNR) at a sampling instant, thereby enabling optimal detection of transmitted symbols in the presence of noise [7]. Its effectiveness relies on precise knowledge of the transmitted pulse shape; the filter must be "matched" to the expected waveform for it to perform optimally. However, in practical systems, especially those involving nonlinear operations such as frequency multiplication, the transmitted pulse shape can be significantly altered, resulting in bandwidth expansion and time-domain distortion. When the receiver applies a matched filter that does not account for these distortions, a situation referred to as mismatched filtering, the consequences can be severe: inter-symbol interference (ISI), loss of spectral components, and a degraded SNR at detection. This misconfiguration undermines the filter's primary function and can lead to substantial performance degradation, particularly when the exact waveform distortion is unknown or hardware-specific and not communicated to the receiver [7].

To the best of our knowledge, this work is the first to investigate blind and adaptive matched filter design at the receiver in the presence of frequency multipliers. We propose an adaptive filtering framework based on Long Short-Term Memory (LSTM) networks, which is a class of recurrent neural networks well-suited for modeling temporal dependencies in time-series data. LSTM-based models have been widely used in applications such as time-series forecasting [8], [9] and noise reduction [10]. Unlike traditional matched filters that rely on fixed, predefined filter design, LSTMs can learn and adapt to evolving spectral and temporal distortions in the received signal. By leveraging their ability to model nonlinear relationships and maintain memory over time, our approach enables dynamic signal reconstruction and effective noise mitigation—independent of the specific frequency multiplier configuration [10]. Our main contributions are summarized as follows:

- We formalize the matched-filter mismatch problem at the receiver arising from the nonlinear behavior of frequency multipliers.
- We propose a novel, data-driven approach utilizing LSTM networks to directly estimate an effective matched filter from the received signal, eliminating the need for pilot symbols or prior knowledge of multiplier characteristics. The proposed method dynamically adapts to varying pulse shapes and bandwidth expansions, thereby providing robust signal reconstruction and effective noise mitigation in the presence of nonlinear distortions.
- Simulation results clearly demonstrate that the proposed LSTM-based matched filter achieves near maximum SNR, in scenarios involving unknown frequency multiplication order. These findings validate its potential for blind receiver design in modern communication systems.

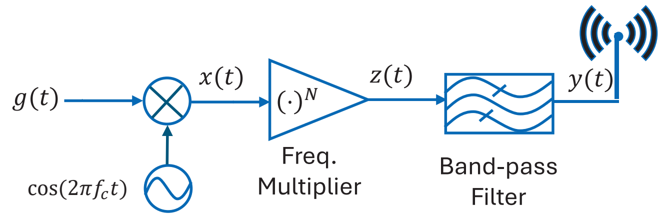

Fig. 1: Transmitter block diagram.

The paper is structured as follows. Sec. II presents the system model and problem formulation. Sec. III describes the LSTM architecture. Sec. IV reports simulation results and performance evaluation. Sec. V concludes the paper.

II. System Model

A. Frequency multiplier input-output relation

The transmitter communication chain incorporating a frequency multiplier is illustrated in Fig. 1. Initially, the baseband signal is up-converted to an intermediate frequency using a mixer. The resulting output then passes through an N-fold frequency multiplier, replacing the multiple cascaded mixers typically employed at lower frequencies. Finally, a bandpass filter suppresses unwanted harmonics, ensuring the transmitted signal remains concentrated around the desired carrier frequency.

The input to the frequency multiplier $x(t)$ is a low-frequency modulated signal, with bandwidth β. The input signal over a symbol period can be expressed as:

$$x(t) = g(t)\cos(2\pi f_c t). \tag{1}$$

Here, $g(t)$ denotes the pulse shape/expression with pulse width $T \propto \frac{1}{\beta}$, and f_c refers to the carrier frequency before the multiplier. Given the input signal $x(t)$, the response of the nonlinear circuit can be expressed as:

$$z(t) = \sum_{n=1}^{N} a_n x^n(t) = \sum_{n=1}^{N} a_n g^n(t)\cos^n(2\pi f_c t), \tag{2}$$

where $\{a_n, n = 1, 2, \cdots, N\}$ are the coefficients of the nonlinear circuit's response. By expanding and then grouping the terms according to their harmonics, the output signal expression becomes:

$$\begin{aligned} z(t) &= \sum_{n=0}^{N} b_n(t)\cos(2\pi n f_c t) \\ &= \sum_{n=0}^{N-1} b_n(t)\cos(2\pi n f_c t) + c\, g^N(t)\cos(2\pi N f_c t). \end{aligned} \tag{3}$$

The term involving the harmonic $\cos(2\pi N f_c t)$ is a scalar multiple of $g^N(t)$, representing the N-th harmonic contribution to the signal. The remaining terms, denoted by $\{b_n(t), n \neq N\}$, are polynomial functions of $g(t)$, capturing the contributions from other harmonics. Here, c is a random constant that encompasses the modulated symbol value. To elaborate, consider the case of a frequency quadruple, i.e., $N = 4$. In this case, the output expression becomes:

$$\begin{aligned} z(t) = &\left(\frac{a_2 g^2(t)}{2} + \frac{3a_4 g^4(t)}{8}\right) \\ &+ b_1(t)\cos(2\pi f_c t) + b_2(t)\cos(2\pi(2f_c)t) \\ &+ b_3(t)\cos(2\pi(3f_c)t) + b_4(t)\cos(2\pi(4f_c)t), \end{aligned} \tag{4}$$

where:

$$b_1(t) = a_1 g(t) + \frac{3a_3}{4}g^3(t), b_2(t) = \frac{a_2}{2}g^2(t) + \frac{a_4}{2}g^4(t),$$
$$b_3(t) = \frac{a_3}{4}g^3(t), \quad b_4(t) = \frac{a_4}{8}g^4(t).$$

The last term in (4) is the dominant contribution from the fourth harmonic, and the sum represents the additional harmonic, each modulated by polynomial functions of $g(t)$.

The output of the nonlinear device is a linear combination of modulated harmonics. Since the coefficients are polynomial functions of $g(t)$, the bandwidth associated with each harmonic is no longer equal to the original bandwidth β. This effect is known as pulse distortion and it induces bandwidth expansion as a result of N-fold convolutions in the frequency domain [2]. Band-pass filtering around the highest harmonic modulated signal, the signal over one symbol period can be expressed as:

$$y(t) = c\, g^N(t)\cos(2\pi N f_c t). \tag{5}$$

B. The case of Sinc pulse

To elaborate on the pulse distortion, we consider the Sinc pulse as an example. The frequency multiplier input signal expression, over one symbol period, is given by [11]:

$$x_s(t) = A\frac{\sin(\pi t/T)}{\pi t/T}\cos(2\pi f_c t), \tag{6}$$

where T is the symbol period. Accordingly, the output signals after filtering is given by:

$$y_s(t) = cA^N\frac{(\sin(\pi t/T))^N}{(\pi t/T)^N}\cos(2\pi N f_c t). \tag{7}$$

Recall that c takes random value each symbol period, encompassing the value of the modulated symbol.The Fourier transform of Sinc pulse gives a rectangular function with a width equal to $\frac{1}{T}$:

$$T\mathrm{rect}_{\frac{1}{T}}(f) = \begin{cases} T, & \text{if} \quad |f| \le \dfrac{1}{2T} \\ 0, & \text{else where.} \end{cases} \tag{8}$$

The frequency representation of the frequency multiplier output signal is N-times convolution of rectangular function (multiplication in time domain is equivalent to convolution in the frequency domain)

$$Y_s(f) = T_c^N \mathrm{rect}^{*N}_{\frac{1}{T}}(f) * \frac{\delta(f - Nf_c) + \delta(f + Nf_c)}{2}. \tag{9}$$

Here $\mathrm{rect}^{*N}(f)_{\frac{1}{T}}$ denotes the N-times convolution of the rectangular function. The N-fold convolution of rectangular functions yields a piecewise polynomial function of degree $N-1$. For example, in the case of a tripler, we have:

$$\mathrm{rect}^{*3}_{\frac{1}{T}}(f) = \begin{cases} 0, & |f| > \frac{3}{2T} \\ \frac{1}{2}\left(\frac{1}{T}\right)^2\left(f + \frac{3}{2T}\right)^2, & -\frac{3}{2T} \le f < -\frac{1}{2T} \\ \frac{3}{4}\left(\frac{1}{T}\right)^3 - \left(\frac{1}{T}\right)^2 f^2, & -\frac{1}{2T} \le f < \frac{1}{2T} \\ \frac{1}{2}\left(\frac{1}{T}\right)^2\left(f - \frac{3}{2T}\right)^2, & \frac{1}{2T} \le f \le \frac{3}{2T} \end{cases} \tag{10}$$

The time-domain expression, obtained via the inverse Fourier transform, results in a non-trivial form that varies with the multiplication order N.

C. Matched Filter expression

The transmissions are subject to Additive White Gaussian Noise (AWGN), denoted by $n(t)$, with Power Spectral Density (PSD) equal to ρ. The base-band signal, over one symbol period, can be written as

$$r(t) = cg^N(t) + n(t). \tag{11}$$

The variance of each noise sample before filtering is close to infinity, as it corresponds to the integral of the PSD over the entire frequency domain. Therefore, a matched filter should be applied that will play the role of low pass filter to reduce the effect of the noise and maximize the SNR. Subsequently, a filter with impulse response $h(t)$ is applied to extract and filter the baseband signal.

The derivation of the matched filter begins by considering the filtered version of received signal $r(t)$ as a convolution of the received signal $cg^N(t)$ plus noise $n(t)$ with the filter impulse response $h(t)$:

$$r(t) * h(t) = (cg^N(t) + n(t)) * h(t) \tag{12}$$

The SNR of the sampled version for $t = 0$, can be written as:

$$\mathrm{SNR} := \frac{\left|\int_{-\infty}^{\infty} h(\tau)cg^N(\tau)d\tau\right|^2}{\mathrm{E}[(h(t) * n(t))^2]} \tag{13a}$$
$$= \frac{c^2\left|\int_{-\infty}^{\infty} h(\tau)g^N(\tau)d\tau\right|^2}{\int_{-\infty}^{\infty}|H(\omega)|^2\rho d\omega} \tag{13b}$$
$$\le \frac{c^2\int_{-\infty}^{\infty} g^{2N}(\tau)d\tau\int_{-\infty}^{\infty} h^2(\tau)d\tau}{\rho\int_{-\infty}^{\infty}|H(\omega)|^2 d\omega} \tag{13c}$$
$$= \frac{c^2\int_{-\infty}^{\infty} g^{2N}(\tau)d\tau}{\rho} \tag{13d}$$

The inequality in (13c) follows from the Cauchy–Schwarz inequality and becomes an equality when $h(t) = g^N(t)$, which motivates the notation of the matched filter. This indicates that the SNR is maximized when the receiver filter is matched to the distorted pulse $g^N(t)$, rather than the original baseband pulse $g(t)$. However, practical challenges arise when the received signal includes unknown parameters, such as an

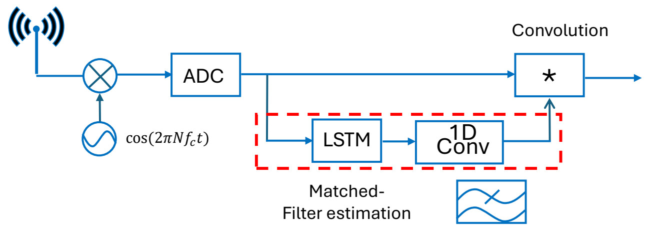

Fig. 2: Receiver structure with integrated LSTM-based filtering.

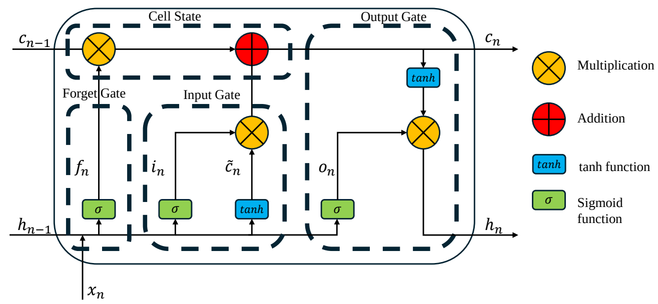

Fig. 3: LSTM Cell Architecture.

unknown frequency multiplication factor N, or when the frequency multiplier is non-ideal, introducing a mismatch factor $N+\alpha$, where α represents uncertainty or hardware-induced noise. Moreover, even when N is known, the output of the frequency multiplier generates non-standard pulse shape that depends heavily on the multiplication order, as demonstrated in (10). These distorted pulses are analytically complex and difficult to generate or model precisely, further complicating the design of an optimal matched filter.

III. LSTM-based Matched Filter Design

A. Receiver Structure

Following the down-conversion process, a copy of the received signal is used for matched filter estimation, as illustrated in Fig. 2. Each input, corresponding to the symbol duration, is utilized to update the matched filter. It is important to note that the received signal is modulated, exhibiting random amplitude, and is further corrupted by noise. The proposed matched filter estimation pipeline consists of two main stages: an LSTM network followed by a one-dimensional convolutional layer. The LSTM network processes the sequential input data to capture long-term temporal dependencies, transforming each input along with previously received signal into a richer, 64-dimensional feature representation. This transformation leverages the LSTM's gating mechanisms and its use of the hyperbolic tangent (tanh) activation function to retain relevant historical patterns.

Subsequently, the one-dimensional convolutional layer performs local feature refinement. With a kernel size of one and a linear activation function, it computes a weighted combination across the 64-dimensional LSTM output, reducing the feature space to a compact, single-dimensional representation. This ensures that the final output remains both computationally efficient for matched filter construction.

B. Adaptive Matched Filter Estimation Using LSTM

The received continuous-time signal is typically sampled by an analog-to-digital converter (ADC), resulting in discrete-time observations. The resulting sampled signal at the receiver, denoted by

$$\boldsymbol{r}[n] = \sum_k c_k g^N(nT_s - KT) + n(nT_s).$$

The sampling period T_s is adjusted to be higher than Nyquist lower bound. The transmitted symbol modulated by a pulse shape (with random amplitude due to modulation) and corrupted by additive noise. Formally, each received symbol period provides a sequence of sampled observations, which serve as inputs to our adaptive matched filter estimation algorithm. The role of the proposed LSTM neural networks is to dynamically estimate the matched filter directly from these sampled sequences. The inherent temporal dependency and nonlinearity present in the received sampled signal make LSTM particularly suitable for modeling the underlying pulse shape.

LSTM networks, an advanced variant of recurrent neural networks (RNNs), incorporate gated mechanisms, forget, input, and output gates, to selectively retain or discard historical information. As depicted in Fig. 3, the LSTM cell processes the sampled input sequence $\boldsymbol{r}[n]$ to update its internal cell state and hidden states. The forget gate assesses which information from previous symbol periods remains relevant, defined as:

$$f_n = \sigma(W_f \cdot [h_{n-1}, \boldsymbol{r}[n]] + b_f), \tag{14}$$

where $\sigma(\cdot)$ denotes the sigmoid function. Values close to 1 indicate retention of prior knowledge, while values near 0 discard less relevant information.

The input gate identifies new information from the current sampled input sequence that should update the internal memory. It computes:

$$i_n = \sigma(W_i \cdot [h_{n-1}, \boldsymbol{r}[n]] + b_i), \tag{15}$$

$$\tilde{C}_n = \tanh(W_C \cdot [h_{n-1}, \boldsymbol{r}[n]] + b_C), \tag{16}$$

generating a candidate update to the cell state based on current signal characteristics. Subsequently, the LSTM cell updates its internal cell state as:

$$C_n = f_n \odot C_{n-1} + i_n \odot \tilde{C}_n, \tag{17}$$

where $\odot$ denotes element-wise multiplication. This adaptive updating captures temporal variations of the pulse shape across consecutive samples.

Lastly, the output gate determines the next hidden state h_n, summarizing information relevant for matched filter estimation:

$$o_n = \sigma(W_o \cdot [h_{n-1}, \boldsymbol{r}[n]] + b_o), \quad h_n = o_n \odot \tanh(C_n). \tag{18}$$

Through these gating mechanisms, the LSTM network effectively extracts and preserves temporal patterns within sampled symbol periods, directly modeling the matched filter's temporal dynamics.

C. Pulse Refinement through One-Dimensional Convolution

While the LSTM provides a temporally rich and high-dimensional representation of the pulse characteristics, we further refine this representation into a more explicit matched filter estimate through a one-dimensional convolutional (1DConv) layer. This convolutional layer performs a learned linear combination across the LSTM output feature dimensions. Specifically, at each sampled time step, the convolutional layer applies a kernel with size one and linear activation to aggregate the 64-dimensional temporal representation provided by the LSTM network. Formally, the matched filter coefficient estimation at each discrete-time index n can be expressed as:

$$\hat{h}[n] = W_{\text{conv}} \cdot h_n + b_{\text{conv}}, \tag{19}$$

where W_{conv} and b_{conv} represent the learned weights and bias of the convolutional operation, respectively. This results in a concise and effective matched filter estimate suitable for matched filtering and subsequent symbol detection.

By combining the adaptive temporal modeling of the LSTM with the localized refinement capabilities of the 1D convolutional layer, our approach provides a fully data-driven solution to the problem of matched filter estimation, robustly handling modulation-induced randomness, hardware imperfections, and unknown distortions encountered in practical communication systems.

IV. Simulation Results

We analyze the performance of the LSTM-based matched filter through extensive numerical simulations, evaluating both the achieved SNR and the Mean Square Error (MSE). For comparison, we consider two benchmark approaches:

- Expanded Bandwidth Filter (EBF) :A wideband version of the matched filter with a compressed time-domain representation (i.e., bandwidth expanded by a factor of N), but based on the same pulse form as $g(t)$. Several recent studies have demonstrated that the signal bandwidth may expand by a factor on the order of N [3].
- Conventional Matched Filter (CMF): The conventional matched filter using the original baseband pulse $g(t)$.

Furthermore, as a natural point of comparison, we consider the ideal case of perfect Matched Filter (MF) reconstruction.

Fig. 4 illustrates the effect of the frequency multiplier on a Gaussian pulse, where $N = 1$ corresponds to the original pulse $g(t)$. As observed, increasing the multiplier order N results in temporal compression of the pulse and a corresponding expansion in the frequency domain. This behavior is consistent with the time-bandwidth product, where compression in one domain leads to expansion in the other.

Training data comprise a comprehensive dataset of computer-generated pulses, including Gaussian and Raised Cosine waveforms. To achieve robust generalization, we vary pulse amplitudes, symbol periods, and SNRs randomly across training samples, while maintaining a fixed pulse shape during each individual transmission scenario. The model is trained for 50 epochs using a batch size of 1000 samples per iteration. We use MSE to quantify the discrepancy between the true transmitted signal samples and the LSTM-predicted outputs, is mathematically defined as:

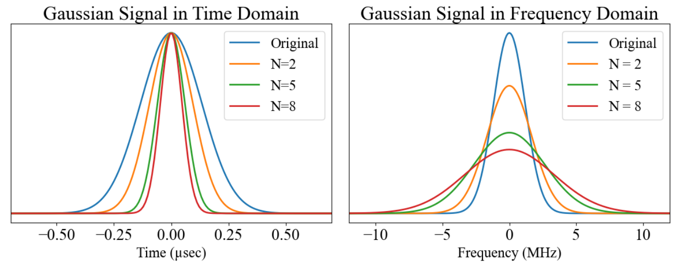

Fig. 4: Time and frequency domain representations of the Gaussian pulse with different multiplier order.

$$\text{MSE} = \frac{1}{N} \sum_{i=1}^{N} \frac{(y_i - \hat{y}_i)^2}{y_i^2}, \tag{20}$$

where y_i denotes the true sampled signal amplitude, $\hat{y}_i$ is the corresponding estimated value produced by the model, and N is the total number of evaluated samples. At the conclusion of training, the model achieves an MSE of 0.0167 on the validation dataset, suggesting effective convergence and satisfactory training generalization.

In the simulations, each waveform is generated with randomized amplitudes to simulate modulation-like variations. A diverse set of pulse shapes and widths is used, including Gaussian and Raised Cosine pulses with varying roll-off factors. Additionally, different frequency multiplication factors, uniformly distributed in the range [2, 10], are applied to ensure diversity within the dataset. The random amplitudes are drawn from a uniform distribution over the interval $[-1, 1]$. To establish a consistent reference, the signal and noise levels are configured such that, under an ideal matched filter (perfect reconstruction of the matched filter), the resulting SNR would be 25 dB. When applying any filtering method, whether the proposed LSTM-based filter or one of the benchmark matched filters, some level of degradation is expected, and the resulting SNR reflects the practical performance of each method under these conditions. For the MSE calculation, a normalized version is used, where the squared error is divided by the squared amplitude range of the signal. This ensures that the MSE values are scale-invariant and comparable across signals with varying amplitudes.

Simulations are conducted using independently generated datasets comprising 100 samples for each waveform type: Gaussian and Raised Cosine pulses. The performance was evaluated in terms of both MSE and SNR. Recall that the a mismatched filter at the receiver results in SNR reduction.

The results for Gaussian pulses are summarized in Table I, and for Raised Cosine pulses in Tab. II.

TABLE I: Performance Comparison for Gaussian Pulses

Filter Type	MSE	SNR (dB)
EBF	0.02205	10.33
CMF	0.17251	1.03
LSTM	0.00234	22.70
Perfect MF	0	25

TABLE II: Performance Comparison for Raised Cosine Pulses

Filter Type	MSE	SNR (dB)
EBF	0.07742	10.00
CMF	0.07743	10.01
LSTM	0.00448	24.70
Perfect MF	0	25

As observed from the tables, the LSTM-based filter consistently outperforms both CMF and EBF baselines in terms of MSE and SNR across both waveform types. The performance gain is particularly significant for Gaussian pulses, where the LSTM achieves an SNR exceeding 22 dB and an MSE of 0.0023, compared to 10.33 dB and 0.0220 for the EBF, and only 1.03 dB and 0.1725 for the CMF. The CMF performs worse than BMF in this case, likely due to temporal misalignment introduced by the bandwidth expansion, which distorts the pulse shape severely when applied to Gaussian waveforms.

In the case of Raised Cosine pulses, the LSTM still achieves superior performance, but the CMF and EBF show nearly identical results. This can be explained by the fact that we are using random roll-off factors during pulse generation. When the roll-off factor is small, the distortion introduced by the frequency multiplier is minimal, and the pulse shape remains relatively unchanged, as illustrated in Fig. 5 for a roll-off factor of 0.4. Conversely, as the roll-off factor increases, the discrepancy between the original and post-multiplier pulse shapes becomes more pronounced. As a result, performance alternates between the CMF and EBF depending on the roll-off value, leading to an overall convergence in their average performance. Nonetheless, the LSTM remains robust across this variability and provides consistently improved results.

These results demonstrate the LSTM model's strong adaptability and its capacity to generalize across waveform structures and noise conditions, offering a flexible and learning-based alternative to traditional matched filtering techniques.

V. Conclusion

In this study, we introduced an adaptive, blind matched-filter estimation approach utilizing a LSTM neural network to effectively address signal distortions caused by nonlinear frequency multipliers in mmWave and sub-THz wireless communication systems. Our proposed method dynamically estimates the matched filter directly from the noisy, modulated received signals, eliminating the need for pilot symbols or prior knowledge of the frequency multiplier configuration. Simulation results validated the high accuracy of our matched filter estimation, achieving a mean-square error with four-decimal precision and near maximum SNR. The adaptive LSTM-based approach demonstrated robustness against spectral and temporal distortions, effectively mitigating inter-symbol interference and preserving signal integrity. Future work will extend the current matched filter estimation framework toward learning-based reconstruction of additional receiver components. This includes exploring AI-driven demodulation and equalization, progressively moving toward a fully trainable receiver chain that adapts to hardware impairments and complex channel dynamics.

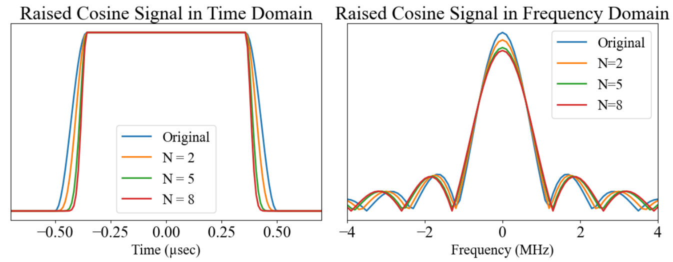

Fig. 5: Time and frequency domain representations of the Raised Cosine signal with different exponentiation factors.

References

[1] S. Kang, S. V. Thyagarajan, and A. M. Niknejad, "A 240 GHz fully integrated wideband QPSK transmitter in 65 nm CMOS," *IEEE J. Solid-State Circuits*, vol. 50, no. 10, pp. 2256–2267, 2015.

[2] A. Darwish, J. Qiu, E. Viveiros, H. A. Hung, and J. Hesler, "Efficient linear transmission of complex waveforms at 216 GHz using nonlinear multiplier chains," in *Proc. IEEE IMS*, 2016.

[3] A. B. Ayed, I. Jaffri, A. M. Darwish, P. Mitran, and S. Boumaiza, "Proof-of-concept of millimeter-wave RF beamforming transmitter architecture employing frequency-multiplier-based up-converters," *IEEE Microw. Wireless Compon. Lett.*, vol. 32, no. 6, pp. 776–779, 2022.

[4] G. C. Tripathi and M. Rawat, "High-frequency signal generator using cascaded frequency multiplier," *IEEE Access*, vol. 11, pp. 74 559–74 568, 2023.

[5] S. V. Thyagarajan, S. Kang, and A. M. Niknejad, "A 240 GHz fully integrated wideband qpsk receiver in 65 nm CMOS," *IEEE J. Solid-State Circuits*, vol. 50, no. 10, pp. 2268–2280, 2015.

[6] A. Chung, A. M. Darwish, E. Viveiros, H. A. Hung, P. Mitran, and S. Boumaiza, "Analysis and compensation of nonidealities in frequency multiplier-based high-frequency vector signal generators," *IEEE Transactions on Microwave Theory and Techniques*, vol. 67, no. 6, pp. 2270–2283, 2019.

[7] J. Proakis, *Digital Communications*, ser. Communications and signal processing. McGraw-Hill, 1989. [Online]. Available: https://books.google.com.tr/books?id=fGbHQgAACAAJ

[8] J. Luo, Z. Zhang, Y. Fu, and F. Rao, "Time series prediction of covid-19 transmission in america using lstm and xgboost algorithms," *Results in Physics*, vol. 27, p. 104462, 2021. [Online]. Available: https://www.sciencedirect.com/science/article/pii/S2211379721005775

[9] A. W. Ghani Rizky Naufal, "Time series forecasting based on deep learning cnn- lstm-gru model on stock prices," *International Journal of Engineering Trends and Technology*, vol. 71, no. 6, pp. 126–133, 2023.

[10] H. Arab, I. Ghaffari, R. M. Evina, S. O. Tatu, and S. Dufour, "A hybrid LSTM-ResNet deep neural network for noise reduction and classification of v-band receiver signals," *IEEE Access*, vol. 10, pp. 14 797–14 806, 2022.

[11] M. Cavallaro, T. Copani, and G. Palmisano, "A Gaussian pulse generator for millimeter-wave applications," *IEEE Trans. Circuits Syst. I*, vol. 57, no. 6, pp. 1212–1220, 2009.